Analyzing a Resonant Switched-Capacitor Converter for Improving Lithium-Ion Battery Cells Balancing Speed

Shahin Goodarzi[1], Reza Beiranvand[2*], and Mustafa Mohamadian[3]

Abstract

Active techniques based on the switched-capacitor converters (SCCs) are used in recent years widely for battery cell balancing applications, due to lack of bulky magnetic components. In addition, these converters are easily be integrated to reduce the volume. Despite of all these benefits, SCCs have some disadvantages such as number of active switches, currents spikes, low balancing speed, and high switching losses. In this paper, a chain resonant SCC is analyzed which can realize soft switching under the ZCS conditions to eliminate currents spikes to overcome the aforementioned SCCs drawbacks. Also, it has been modified to increase balancing speed of the Lithium-Ion battery cells. Then, a chain resonant SCC for balancing a combination of three battery cells with capacity of 2150 mAh and nominal voltage of 3.6 V has been simulated by MATLAB/SIMULINK and it has been implemented at 50 kHz to confirm operation of the converter. The simulation and experimental results are in good agreement with the given mathematical analyses and illustrate that the balancing speed has been improved more than three-fold, as compared with the conventional converter.

I. INTRODUCTION

LITHIUM-Ion battery cells are one of the most suitable rechargeable batteries which are used widely in industries due to their valuable advantages such as: high energy density and low self-discharge rate [1]-[14]. Generally, several batteries are connected in series, in practice, to prepare the required loads voltages. Therefore, they [1]are charged and discharged in series connections at the same times [3], [26]. In these applications, repeating the charge and discharge processes in long time intervals in addition to some unavoidable practical mismatches in the batteries chemical and electrical characteristics such as: production variety, unbalanced aging, and temperature distribution, cause some issues. To overcome these problems, the Lithium-Ion battery cells should be protected from overvoltage and under voltage rates. So, there should be balancing circuits to avoid the unpredicted events. The balancing circuits overcome these unavoidable mismatches, significantly. They also, enhance total capacity, improve efficiency, and increase batteries lifetimes, significantly [4], [18]-[30].

Different balancing circuits have been introduced in the literature in recent years, which can be categorized in two separated groups: 1) passive, and 2) active. The passive balancing circuits have some disadvantages such as energy loss and thermal problems [2]-[20]. To overcome these issues, active balancing circuits have been introduced, recently, by employing active elements such as inductors and capacitors in their constructions [2], [15]-[20].

Usually two types of active converters are used for balancing battery cells applications [1], [22]-[29]: 1) Switched-capacitor based converters and 2) Inductor based converters. Different circuits based on the inductive approach have been introduced in literature [5]-[8]. But, these circuits have large sizes, high cost, and excess losses. Therefore, switched-capacitor topologies have been introduced for balancing battery cells owing to the fact that they do not use bulky magnetic elements such as inductors and transformers. These topologies are much more compact and can be implemented, easier in practice [1], [12], and [13]. But, the SCCs have some problems in the battery cells balancing applications: 1) balancing battery cells needs more time in comparison with the inductor based converters, especially when number of the cells is increased [1], 2) switching losses are high due to hard switching events [2]-[20], and 3) the circuit currents have excessive spikes[1].To increase speed of the SCC based balancing circuits, lots of researches have been

MSc Student, Department of Electrical Engineering, School of Engineering, Tarbiat Modares University, Tehran, Iran,
[2]Assistant Professor, of Electrical Engineering,, Tarbiat Modares University, Tehran, Iran

[3]Associate Professor, of Electrical Engineering,, Tarbiat Modares University, Tehran, Iran

done, recently. Double-tiered SCC has been introduced in [1], [11]. This approach reduces the balancing time, strikingly, by employing additional bridging. However, due to different gradients of the ambient temperature, risks of unbalancing between the outer cells are increased, normally [1]. In addition, this method is unusable for increasing higher balancing speeds. To improve performance by increasing the speed especially between outer cells, two circuits with chain structure have been studied in [1]. Decrease of the farthermost cells to half is one of the advantages of this circuit [1]. Therefore, the cells balancing speed are significantly increased by this chain structure.

As mentioned above, other main problem of the SCCs is due to limitation on accessible size of storage elements and dependence of their sizes on switching frequency causes to increase switching frequency, and it will increase the switching loss due to hard switching events. To overcome this problem, the resonant SCCs have been introduced [1]-[14]. The performance analysis of complex SCCs is introduced in [1]-[3]. Specifically, a resonant SCC has been used for voltage balancing of series-connected capacitor in [2]. Although chain structure SCC [1] has high cells balancing speed, there are some problems such as high number of switches and hard switching events that increases the switching losses. A chain structure resonant SCC with zero-current switching (ZCS) technique is introduced in this paper. This configuration is suitable for series connected battery or super capacitor strings to achieve zero-voltage gap. High balancing speed, zero voltage gap among the cells, low current spikes, and low switching losses are main advantages of this converter. In Sec. II the conventional resonant switched-capacitor converter has been modified. In Sec. III the converter different operation modes have been analyzed. In Sec. IV the converter balancing time and efficiency have been calculated. In Sec. V the conventional resonant SCC balancing speed has been analyzed. Two converters charge transfer average steps have been compared in Sec. VI. Simulation and experimental results are given in sections VII and VIII, respectively. Finally, conclusion is made in Sec. IX.

NOMENCLATURE

C_{ab} Common capacitor
C_r Capacitance of the resonant capacitor
C_{batt} Capacitance of battery
$E_{Im.}$ Unbalanced energy before cell balancing
$E_{Res.}$ Remained energy of $E_{Im.}$ after cell balancing
f_s Switching frequency

f_r Resonant frequency
i_{L_r} Resonant inductor's current
i_B Battery average current
L_r Resonant inductor
N Number of batteries
P Power transfer rate
P_{Loss} Power losses
Q Quality factor
R_{sw} Switch resistance
R_{Limit} Inrush current limiting resistor
R_C Equivalent resistance of the PCB tracks, switches, inductors, and resonant capacitor
T_{EQ} Balancing time
$V_{C_{ab}}$ Voltage of the common capacitor
V_{Lab} Resonant inductor voltage
V_{B1-4} Voltages of cells 1-4
V_{Bi_start} Cell voltage of ith cell before cell balancing
V_{Bi_end} Cell voltage of ith cell after cell balancing
V_{min} Minimum voltage before cell balancing
V_d Voltage drop on each switch
W Stored energy in the resonant tank's capacitor
ρ Damping ratio
η Power conversion efficiency

II. MODIFYING THE CONVENTIONAL RESONANT SWITCHED-CAPACITOR CONVERTER

A conventional resonant SCC for balancing battery cells is given in Fig. 1 (a). There are four switches in this converter which are controlled simultaneously at a constant switching frequency. Also, switches are connected to up and down battery cells approximately with a duty cycle of 50% by considering short dead-time intervals. There are two different operation modes, as illustrated in Fig. 1 (b) and (c). The conventional resonant SCC has low balancing speed despite of its high efficiency, low switching loss, and low edge current.
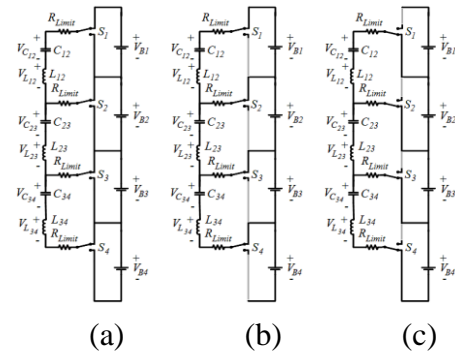

Fig. 1 Conventional resonant SCC [2] (a) circuit topology, (b) mode I, and (c) mode II

Here, the conventional resonant SCC has been modified which has higher balancing speed in comparison with the conventional resonant SCC. Also, all switches are turned off under the ZCS condition, too. The modified converter consists of two sections: 1) resonant tank networks for saving and transferring energy and 2) switches network for connecting the battery cells to the resonant tanks, as shown in Fig. 2.
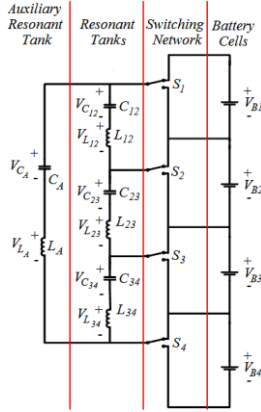
**Fig. 2** The modified converter with an additional resonant tank network

III. ANALYZING THE CONVERTER DIFFERENT OPERATION MODES

To simplify analyses of the circuit and describing its operation modes, it is assumed that there are two battery cells in the string, and the upper cell voltage is higher than the lower cell one, as shown in Fig. 3. The modified section is used when more than two battery cells are connected in series. So, for two battery cells, as shown in Fig. 3, there is no additional resonant tank circuit. The given analyses can be generalized for n battery cells, easily. Here, switching frequency is chosen smaller than the converter resonant frequency to achieve ZCS soft switching under the DCM operation mode and to equalize the battery cells voltages, easily without applying any closed loop control:

$$f_s \leq f_r = \frac{1}{2\pi\sqrt{L_r C_r}},\tag{1}$$

The converter different operation modes are given in Fig. 3. Mode *I* or energy saving mode [t_0-t_1]: switches S_1 and S_3 are turned on during this operation mode to connect the resonant tank to the upper battery cell. Current flows through the resonant capacitor to increase its voltage to maximum value. The equivalent circuit during this operation mode has been plotted in Fig. 3 (a). When the resonant inductor current i_{L_r}, reaches to zero, S_1 and S_2 are turned off

under the ZCS condition. Typical current and voltage waveforms of the proposed circuit are illustrated in Fig. 4.
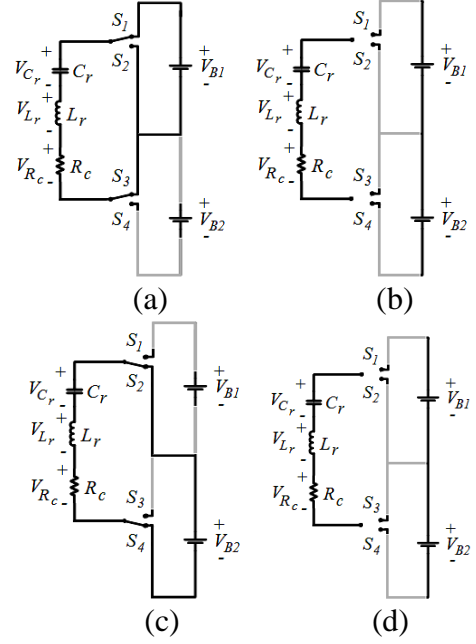
Fig. 3 Circuit different operation modes (a) mode *I* or energy store mode, (b) mode II, (c) mode *III* or energy release mode, and (d) mode IV
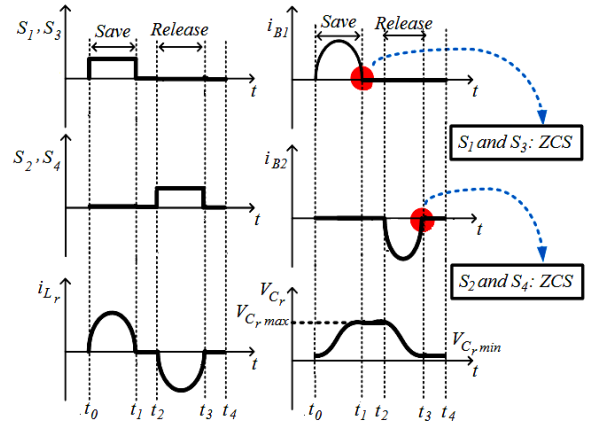
Fig. 4 Typical current and voltage waveforms of the converter during a switching period

Considering Figs. 3 and 4, we can write:

$$\begin{cases} V_{B1} = v_{C_r}(t) + L_r \dfrac{di_{C_r}(t)}{dt} + R_c i_{C_r}(t), \\[2mm] i_{C_r}(t) = C_r \dfrac{dv_{C_r}(t)}{dt}, \\[2mm] \dfrac{dv_{C_r}(t)}{dt}\Big|_{t=0^-} = 0, \\[2mm] v_{C_r}(t)\big|_{t=0^-} = v_{C_r}(0^-), \end{cases}\tag{2}$$

Doing some simple calculations, resonant capacitor voltage in Laplace domain is given:

43

$$V_{C_r}(s) = \frac{V_{B1}}{s} + \left(v_{C_r}(0) - V_{B1}\right)\left(\frac{s + \rho}{(s + \rho)^2 + \omega_0^2}\right.$$
$$\left. + \frac{\rho}{(s + \rho)^2 + \omega_0^2}\right), \qquad (3)$$

Where,

$$\begin{cases} \omega_0 = \sqrt{\dfrac{1}{L_r C_r} - \left(\dfrac{R_c}{2L_r}\right)^2}, \\ \rho = \dfrac{R_c}{2L_r}, \end{cases} \qquad (4)$$

Now, the resonant capacitor voltage during operation mode *I* can be expressed as follows in time domain:

$$v_{C_r}(t) = V_{B1} - \left(V_{B1} - v_{C_r}(0)\right)\left(\cos \omega_0 t \right.$$
$$\left. + \frac{\rho}{\omega_0} \sin \omega_0 t\right)e^{-\rho t}, \ 0 \le t \le \frac{\pi}{\omega_0} \qquad (5)$$

Also, from (2) resonant inductor current can be identified in Laplace domain, as follows:

$$I_{L_r}(s) = \left(\frac{V_{B1} - v_{C_r}(0)}{\omega_0 L_r}\right)\frac{\omega_0}{(s + \rho)^2 + \omega_0^2}, \qquad (6)$$

Therefore, the resonant inductor current during operation mode *I* is obtained in time domain:

$$i_{L_r}(t) = \left(\frac{V_{B1} - v_{C_r}(0)}{\omega_0 L_r}\right)e^{-\rho t}\sin \omega_0 t, \ 0 \le t < \frac{\pi}{\omega_0} \qquad (7)$$

When the resonant inductor current reaches to zero this operation mode is finished and maximum value of the resonant capacitor voltage is occurred:

$$v_{C_r}\left(t = \frac{\pi}{\omega_0}\right) = V_{B1} + \left(V_{B1} - v_{C_r}(0)\right)e^{-\pi\rho/\omega_0}, \qquad (8)$$

Mode *II* [t_1-t_2]: The equivalent circuit during this operation mode has been plotted in Fig. 3 (b). During this operation mode, all power switches are off and DCM operation mode is occurred. Thus, the capacitor voltage is remained constant at its maximum value and the inductor current is equal to zero. So, the resonant capacitor voltage and inductor current are given as follows:

$$\begin{cases} v_{C_r}(t) = V_{B1} + \left(V_{B1} - v_{C_r}(0)\right)e^{-\pi\rho/\omega_0}, \ \dfrac{\pi}{\omega_0} \le t < \dfrac{T_s}{2} \\ i_{L_r}(t) = 0, \end{cases} \qquad (9)$$

Mode *III* or energy releasing mode [t_2-t_3]: switches S$_2$ and S$_4$ are turned on during this operation mode to connect the resonant tank to the lower battery cell. Equivalent circuit of the converter during this operation mode is given in Fig. 3 (c). When the resonant inductor current become zero, S$_2$ and S$_4$ are turned off under the ZCS condition. This operation mode can be analyzed in a similar approach as done in operation mode *I*. Considering $T_s/2$ delay time, the resonant capacitor initial voltage value of $v_{C_r}(T_s/2)$ instead of $v_{C_r}(0)$, and V_{B2} instead of V_{B1}, the resonant capacitor voltage and inductor current values are identified respectively by considering (5) and (7) as follows:

$$v_{C_r}(t) = V_{B2} + \left(v_{C_r}(T_s/2)\right.$$
$$\left. - V_{B2}\right)e^{-\rho(t-T_s/2)}\left(\cos \omega_0(t - T_s/2)\right.$$
$$\left. + \frac{\rho}{\omega_0}\sin \omega_0(t - T_s/2)\right), \quad \frac{T_s}{2} \le t$$
$$< \frac{T_s}{2} + \frac{\pi}{\omega_0} \qquad (10)$$

$$i_{L_r}(t) = \left(\frac{V_{B2} - v_{C_r}(T_s/2)}{\omega_0 L_r}\right)e^{-\rho(t-T_s/2)}\sin \omega_0(t$$
$$- T_s/2), \quad \frac{T_s}{2} \le t < \frac{T_s}{2} + \frac{\pi}{\omega_0} \qquad (11)$$

Where, $v_{C_r}(T_s/2)$ or initial condition is identified from (9),

$$v_{C_r}(T_s/2) = V_{B1}$$
$$+ \left(V_{B1} - v_{C_r}(0)\right)e^{-\pi\rho/\omega_0}, \qquad (12)$$

Mode *IV* [t_3-t_4]: The equivalent circuit during this operation mode has been plotted in Fig. 3 (d). Similar to operation mode *II* all power switches are off. The resonant capacitor voltage is remained constant at its minimum value and the inductor current is equal to zero:

$$\begin{cases} v_{C_r}(t) = V_{B1} + \left(V_{B1} - v_{C_r}(0)\right)e^{-\pi\rho/\omega_0}, \ \dfrac{T_s}{2} + \dfrac{\pi}{\omega_0} \le t < T_s \\ i_{L_r}(t) = 0, \end{cases}$$
$$(13)$$

Under the quasi steady state condition, resonant capacitor voltage values at beginning and end of each switching period are approximately equal, i.e., $v_{C_r}(T_s) \approx v_{C_r}(0)$. Therefore, from (5) and (13) the resonant capacitor initial voltage value is obtained:

$$v_{C_r}(0) = \frac{V_{B2} - V_{B1}e^{-\pi\rho/\omega_0}}{1 + e^{-\pi\rho/\omega_0}}, \qquad (14)$$

Ignoring a special case (i.e., $V_{B2} = V_{B1}$ and $R_C = 0$), the resonant capacitor initial voltage is generally not equal to zero, as can be concluded from (14). Substituting (14) into (7) and (11), resonant inductor current values during operation modes *I* and *III* are respectively rewritten as follows:

$$i_{L_r}(t) = \frac{V_{B1} - V_{B2} + 2V_{B1}e^{-\pi\rho/\omega_0}}{\omega_0 L_r(1 + e^{-\pi\rho/\omega_0})}e^{-\rho t}\sin \omega_0 t, \ 0 \le t \le \frac{\pi}{\omega_0}$$
$$(15)$$

$$i_{L_r}(t)$$
$$= \left(\frac{V_{B2} - V_{B1} + \left(v_{C_r}(0) - V_{B1}\right)e^{-\pi\rho/\omega_0}}{\omega_0 L_r}\right)e^{-\rho(t-T_s/2)}\sin\omega_0(t$$
$$- T_s/2), \quad \frac{T_s}{2} \le t < \frac{T_s}{2} + \frac{\pi}{\omega_0} \qquad (16)$$

Resonant inductor current rms value during operation mode *I* can be calculated as follows:

$$i_{L_r rms-I} = \sqrt{\frac{1}{T_s}\int_0^{\pi/\omega_0} I^2 e^{-2\rho t}\sin^2\omega_0 t\, dt}\ , \qquad (17)$$

To calculate (17), following well-known equations must be considered:

$$\begin{cases} \int \cos ax\, e^{bx}dx = \dfrac{e^{bx}}{a^2+b^2}(a\sin ax + b\cos ax) + C, \\ \sin^2 x = \dfrac{1-\cos 2x}{2}, \end{cases} \qquad (18)$$

Substituting (14) into (7) and doing some algebraic calculations the resonant inductor current rms value during operation mode *I* can be expressed as follows:

$$i_{L_r rms-I} = \sqrt{\frac{f_s C_r}{2R_C}\Delta V_1^2(1 - e^{-2\pi\rho/\omega_0})}, \qquad (19)$$

Where,

$$\Delta V_1 = V_{B1} - v_{C_r}(0), \qquad (20)$$

Also, resonant inductor current rms value during operation mode *III* is written as follows in a same manner:

$$i_{L_r rms-III} = \sqrt{\frac{f_s C_r}{2R_C}\Delta V_2^2(1 - e^{-2\pi\rho/\omega_0})}, \qquad (21)$$

Where,

$$\Delta V_2 = V_{B2} - v_{C_r}\left(\frac{T_s}{2}\right), \qquad (22)$$

From (19) and (21), the resonant inductor current rms value is expressed as follows, easily:

$$\begin{cases} i_{L_r rms} = \sqrt{\dfrac{f_s C_r}{2R_C}(1 - e^{-2\pi\rho/\omega_0})(\Delta V_1^2 + \Delta V_2^2)}, \\ \Delta V_1 = V_{B1} - v_{C_r}(0) = \dfrac{V_{B1} - V_{B2} + 2V_{B1}e^{-\pi\rho/\omega_0}}{1 + e^{-\pi\rho/\omega_0}}, \\ \Delta V_2 = V_{B2} - v_{C_r}\left(\dfrac{T_s}{2}\right) = V_{B2} - V_{B1} - \Delta V_1 e^{-\pi\rho/\omega_0}, \end{cases} \qquad (23)$$

IV. CALCULATING THE BALANCING TIME AND CONVERTER EFFICIENCY

The stored energy in the resonant capacitor during operation mode *I* is given as follows:

$$W = \frac{1}{2}C_r\left(v_{C_r}^2\left(\frac{\pi}{\omega_0}\right) - v_{C_r}^2(0)\right), \qquad (24)$$

Substituting (8) and (14) into (24) and doing some algebraic calculations the stored energy in the resonant capacitor during this operation mode is rewritten:

$$W = \frac{1}{2}C_r(V_{B1} - V_{B2})\left[V_{B1}\left(1 + e^{-1.5\pi\rho/\omega_0}\operatorname{sech}\left(\frac{\pi\rho}{2\omega_0}\right)\right)\right.$$
$$\left. + V_{B2}\tanh\left(\frac{\pi\rho}{2\omega_0}\right)\right], \qquad (25)$$

Some part of this stored energy is dissipated during the energy release mode. From (21), the dissipated power is calculated:

$$P_{Loss-III} = R_C I_{L_r rms-III}^2$$
$$= f_s C_r \Delta V_2^2 e^{-\pi\rho/\omega_0}\sinh\left(\frac{\pi\rho}{\omega_0}\right) \qquad (26)$$

Considering the total stored energy in the resonant capacitor and the dissipated power during operation mode *III*, power transfer rate from resonant capacitor to the battery cell is achieved:

$$P = \frac{W}{T_s} - P_{Loss-III}$$
$$= f_s C_r\left\{\left(\frac{V_{B1} - V_{B2}}{2}\right)\left[V_{B1}\left(1 + e^{-1.5\pi\rho/\omega_0}\operatorname{sech}\left(\frac{\pi\rho}{2\omega_0}\right)\right)\right.\right.$$
$$\left. + V_{B2}\tanh\left(\frac{\pi\rho}{2\omega_0}\right)\right]$$
$$\left. - \Delta V_2^2 e^{-\pi\rho/\omega_0}\sinh\left(\frac{\pi\rho}{\omega_0}\right)\right\} \qquad (27)$$

On the other hand, by considering the full and poor charged battery cells energy values, balancing the battery cells lasts until these two cells' charge become equal. Thus, amount of the transferred energy is:

$$\Delta E = \frac{E_1 - E_2}{2} - \frac{R_C I_{L_r rms}^2}{f_s}, \qquad (28)$$

Also, by considering the full and poor charged battery cell voltage values, these cells' energy values are identified by the following equations:

$$\begin{cases} E_1 = \dfrac{1}{2}C_{cell}V_{B1}^2, \\ E_2 = \dfrac{1}{2}C_{cell}(V_{B1} - \Delta V)^2, \end{cases} \qquad (29)$$

From (28), the transferred energy is given:

$$E_1 - E_2 = \frac{1}{2}C_{cell}[V_{B1}^2 - (V_{B1} - \Delta V)^2] = C_{cell}V_{B1}\Delta V \qquad (30)$$

$$\Delta E = \frac{1}{2}C_{cell}V_{B1}\Delta V - \frac{R_C I_{L_r rms}^2}{f_s} \qquad (31)$$

Average value of the balancing time can be expressed approximately as follows by considering (27) and (31):

$$T_{EQ\,av.} = \frac{\Delta E}{P} = \frac{1}{P}\left(\frac{1}{2}C_{cell}V_{B1}\Delta V\right.$$
$$\left. - C_r(\Delta V_1^2 + \Delta V_2^2)e^{-\pi\rho/\omega_0}\sinh\left(\frac{\pi\rho}{\omega_0}\right)\right) \qquad (32)$$

Power rating parameter specifies the balancing time and power conversion efficiency. Power rating should

45

be high enough to decrease the balancing time value as can be concluded from (32). But, efficiency is reduced by increasing the power rating. Thus, a tradeoff between these two parameters should be done. Assuming the equivalent resistance of the PCB tracks, switches, inductors, and resonant capacitor R_C, the power losses is given:

$$P_{LOSS} = R_C(i_{L_r rms_I}^2 + i_{L_r rms_{III}}^2) = f_s C_r(\Delta V_1^2 + \Delta V_2^2) \quad (33)$$

Besides, the relationship between losses and transferred power to the resonant capacitor can be achieved as follows:

$$P_{LOSS} = \frac{2\pi e^{\pi\rho/\omega_0}}{\omega_0 C_r V_{B1}^2} \tanh\left(\frac{\pi\rho}{2\omega_0}\right) \operatorname{sech}^2\left(\frac{\pi\rho}{2\omega_0}\right) P, \quad (34)$$

Thus, the power conversion efficiency is obtained by considering (34):

$$\eta = \frac{P - P_{LOSS}}{P}$$
$$= 1 - \frac{2\pi e^{\pi\rho/\omega_0}}{\omega_0 C_r V_{B1}^2} \tanh\left(\frac{\pi\rho}{2\omega_0}\right) \operatorname{sech}^2\left(\frac{\pi\rho}{2\omega_0}\right) P \quad (35)$$

So, the conversion efficiency is decreased linearly by increasing the power rating. Thus, although higher power ratings cause higher balancing speeds, but, it reduces the converter efficiency value. Therefore, tradeoff between balancing speed and efficiency must be done, in practice. It should be mentioned that when more than two battery cells are connected in series the same analyses can be done to calculate currents, voltages, and power losses of the converter for each resonant tank network, as done for two battery cells in sections *III* and *IV*. Also, when the modified resonant tank is included for increasing balancing speed of the converter for using more than two battery cells, V_{B_H} and V_{B_L} must be used respectively instead of V_{B1} and V_{B2}:

$$\begin{cases} V_{B_H} = \sum_{i=1}^{N-1} V_{Bi} \\ V_{B_L} = \sum_{i=2}^{N} V_{Bi} \end{cases} \quad (36)$$

V. BALANCING SPEED OF THE CONVENTIONAL RESONANT SCCs

In the conventional resonant SCC, given in Fig. 1, when voltages of the two adjacent cells are different, the charge transfer between these cells is conducted by the common capacitor C_{ab}, for balancing the cells. The balancing speed is slow especially when the number of cells is increased, because in this converter charge is transferred cell by cell. Common capacitor between two cells is connected to upper and lower cells with a unique duty cycle. Voltage of this common capacitor $V_{C_{ab}}$, can be calculated, easily. In the first switching subinterval the capacitor voltage is:

$$V_{C_{ab}} = V_{Ba} - V_{Lab} \quad (37)$$

In the second subinterval the capacitor voltage is equal to:

$$V_{C_{ab}} = V_{Bb} - V_{Lab} \quad (38)$$

Considering (37) and (38) and averaging these two voltage values, the capacitor average voltage value is identified:

$$\langle V_{C_{ab}} \rangle_{T_s} = \frac{1}{T_s}\left(\int_0^{T_s/2} V_{C_{ab}} dt + \int_{T_s/2}^{T_s} V_{C_{ab}} dt\right)$$
$$= \frac{1}{T_s}\left(\int_0^{T_s/2} (V_{Ba} - V_{Lab}) dt + \int_{T_s/2}^{T_s} (V_{Bb} - V_{Lab}) dt\right), \quad (39)$$

Inductor average voltage is equal to zero, because the inductor current values at the beginning and end of the switching period are equal, i.e.,

$$i_L(T_s) = i_L(0) \Rightarrow \langle V_L \rangle_{T_s} = \frac{1}{T_s}\int_0^{T_s} V_L(t) dt = 0 \quad (40)$$

Combination of (37)-(39) yields:

$$\langle V_{C_{ab}} \rangle_{T_s} = \frac{V_{Ba} + V_{Bb}}{2}, \quad (41)$$

Each cell is connected to the common capacitor just during one subinterval. So, the average current entering to the batteries is calculated as follows:

$$\langle i_{Ba} \rangle_{T_s} = \frac{1}{R_{eq}}\left(\frac{V_{Ba} + V_{Bb}}{2} - \left(\frac{1}{T_s}\int_0^{T_s} V_{Lab}(t) dt\right) - V_{Ba}\right)$$
$$= \frac{V_{Bb} - V_{Ba}}{2R_{eq}}, \quad (42)$$

Also, in the second switching subinterval, batteries average current is equal to:

$$\langle i_{Bb} \rangle_{T_s} = \frac{1}{R_{eq}}\left(\frac{V_{Ba} + V_{Bb}}{2} - \left(\frac{1}{T_s}\int_0^{T_s} V_{Lab}(t) dt\right) - V_{Bb}\right)$$
$$= \frac{V_{Ba} - V_{Bb}}{2R_{eq}}, \quad (43)$$

According to (42) and (43) each cell current is related to the equivalent resistor and the existing voltage difference between the two cells. To simplify the calculations it is assumed that the most upper cell voltage value is bigger than the other cells voltages:

$$V_{B1} > V_{B2} = V_{B3} = V_{B4}, \quad (44)$$

Considering Fig. 1, we can write:

$$
\begin{bmatrix} V_{B1} - V_{C12} - \dfrac{1}{T_s}\displaystyle\int_0^{T_s} V_{L12}(t)dt \\ V_{B2} - V_{C23} - \dfrac{1}{T_s}\displaystyle\int_0^{T_s} V_{L23}(t)dt \\ V_{B3} - V_{C34} - \dfrac{1}{T_s}\displaystyle\int_0^{T_s} V_{L34}(t)dt \\ 0 \end{bmatrix} = \begin{bmatrix} (V_{B1}-V_{B2})/2 \\ 0 \\ 0 \\ 0 \end{bmatrix}
$$

$$
= \begin{bmatrix} 2R_{eq}+r_p & -R_{eq} & 0 & 0 \\ -R_{eq} & 2R_{eq}+r_p & -R_{eq} & 0 \\ 0 & -R_{eq} & 2R_{eq}+r_p & 0 \\ 0 & 0 & 0 & 0 \end{bmatrix} \cdot \begin{bmatrix} i_{1A} \\ i_{2A} \\ i_{3A} \\ i_{4A} \end{bmatrix}, \quad (45)
$$

$$
\begin{bmatrix} 0 \\ V_{B2} - V_{C12} - \dfrac{1}{T_s}\displaystyle\int_0^{T_s} V_{L12}(t)dt \\ V_{B3} - V_{C23} - \dfrac{1}{T_s}\displaystyle\int_0^{T_s} V_{L23}(t)dt \\ V_{B4} - V_{C34} - \dfrac{1}{T_s}\displaystyle\int_0^{T_s} V_{L34}(t)dt \end{bmatrix} = \begin{bmatrix} 0 \\ (V_{B2}-V_{B1})/2 \\ 0 \\ 0 \end{bmatrix}
$$

$$
= \begin{bmatrix} 0 & 0 & 0 & 0 \\ 0 & 2R_{eq}+r_p & -R_{eq} & 0 \\ 0 & -R_{eq} & 2R_{eq}+r_p & -R_{eq} \\ 0 & 0 & -R_{eq} & 2R_{eq}+r_p \end{bmatrix} \cdot \begin{bmatrix} i_{1B} \\ i_{2B} \\ i_{3B} \\ i_{4B} \end{bmatrix}, \quad (46)
$$

Here, $r_p = r_b + r_c$. Generally, the batteries balancing current is expressed as follows [1]:

$$
\begin{bmatrix} I_{B1} \\ I_{B2} \\ \cdot \\ \cdot \\ I_{BN-1} \\ I_{BN} \end{bmatrix} = \begin{bmatrix} i_{1A} + i_{1B} \\ i_{2A} + i_{2B} \\ \cdot \\ \cdot \\ i_{(N-1)A} + i_{(N-1)B} \\ i_{NA} + i_{NB} \end{bmatrix}
$$

$$
= \frac{1}{|i_{NB}|} \begin{bmatrix} X(N-1) \\ X(N-2) - X(N-1) \\ \cdot \\ \cdot \\ X(1) - X(2) \\ 0 - X(1) \end{bmatrix}, \quad (47)
$$

Where,

$$
X(N) = \alpha^{N-1} - (N-2)\alpha^{N-3} + \left(\sum_{K=1}^{N-4} K\right)\alpha^{N-5}
$$
$$
- \left(\sum_{M=1}^{N-6}\sum_{K=1}^{M} K\right)\alpha^{N-7} + \cdots, \quad (48)
$$

And,

$$
\alpha = 2 + \frac{r_p}{R_{sw}} \ , \ and \ \sum_{k=1}^{m} k = 0 \quad (m<1) \quad (49)
$$

In Fig. 5, ratio of the balancing current of the farthermost cell to the nearest cell is depicted in terms of number of the cells and resistance ratio (r_p/R_{eq}) [1]. By increasing number of the cells and the resistance ratio, current of the farthest cell is reduced, as illustrated in Fig. 5. Therefore, the conventional resonant switched capacitor balancing circuit has a slow balancing speed when number of cells is increased; in spite of its good efficiency and limited edge current.
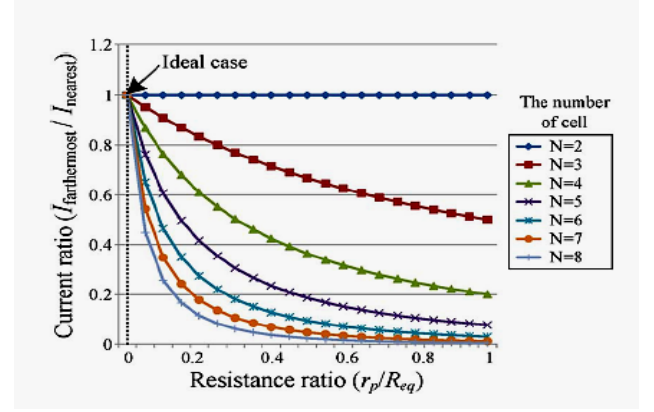
Fig. 5 Balancing current ratio between the nearest cell and the farthermost cell according to the number of cells and resistance ratio [1]

VI. COMPARING TWO CONVERTERS CHARGE TRANSFER AVERAGES STEPS

A comparison between resonant SCC with chain structure and conventional resonant SCC is given, here. When power ratings of both modified and conventional converters are equal, charge transfer average steps is a good parameter for comparing balancing speeds of the converters. Average steps of the charge transfer are identified by calculated the necessary steps for transferring energy from one cell to the other. For simplicity of analysis it is assumed that each battery is composed of N cells connected in series which N is an odd number [1], [2]. Average steps of the charge transfer can be calculated as follows [1], [4]:

$$
Step_{av.} = \frac{\sum Step_{ij-min}}{\#of\ cases}, \quad (50)
$$

Here, $Step_{ij}$ is the minimum steps necessary for charge transfer from cell number i to j, and # of cases is the number of whole steps. Minimum steps for charge transfer from cell i to cell j are given in tables I and II for the conventional and proposed resonant SCCs, respectively. According to table I the whole number of steps and the total number of minimum steps are calculated as follows:

$$
\sum Step_{ij-min} = 2\left(\sum_{K=1}^{N-1}\sum_{i=1}^{K} i\right)
$$
$$
= \sum_{K=1}^{N-1} K(K+1)
$$
$$
= \frac{N(N-1)(N+1)}{3}, \quad (51a)
$$
$$
X = \frac{N-1}{2}, \quad \#of\ cases = N(N-1), \quad (51b)
$$

Thus, the average steps for the conventional resonant SCC is [1]:

$$
Step_{av.} = \frac{1}{3}(N+1), \quad (52)
$$

According to table II the whole number of steps and the total number of minimum steps are calculated as follows:

$$\sum Step_{ij-min} = 2\left(N\sum_{K=1}^{X} K\right) = N * X(X+1)$$
$$= N\left(\frac{N-1}{2}\right)\left(\frac{N+1}{2}\right), \qquad (53a)$$

$$X = \frac{N-1}{2}, \quad \#of\ cases = N(N-1), \qquad (53b)$$

TABLE I. MINIMUM STEPS FOR CHARGE TRANSFER IN THE CONVENTIONAL RESONANT SCC [1]

To cell / From cell	B_1	B_2	...	B_X	...	B_{N-2}	B_{N-1}	B_N
B_1		1	...	X-1	...	N-3	N-2	N-1
B_2	1		...	X-2	...	N-4	N-3	N-2
...	...	...	...	...		...	...	...
B_{N-1}	N-2	N-3	...	X	...	1		1
B_N	N-1	N-2	...	X+1	...	2	1	

TABLE II. MINIMUM STEPS FOR CHARGE TRANSFER IN THE PROPOSED CONVERTER

To cell / From cell	B_1	B_2	...	B_X	...	B_{N-2}	B_{N-1}	B_N
B_1		1	...	X-1	...	3	2	1
B_2	1		...	X-2	...	4	3	2
...	...	...	...	...	...	...	...	...
B_{N-1}	2	3	...	X	...	1		1
B_N	1	2	...	X	...	2	1	

Thus, the average of steps for the proposed converter is:

$$Step_{av.} = \frac{(N+1)}{4}, \qquad (54)$$

In Fig. 6, the average steps for charge transfer in each converter are depicted. It can be seen that the modified converter has lower average steps than the conventional converter. Thus, it can be concluded that balancing speed of the modified converter is higher than the balancing speed of the conventional converter.
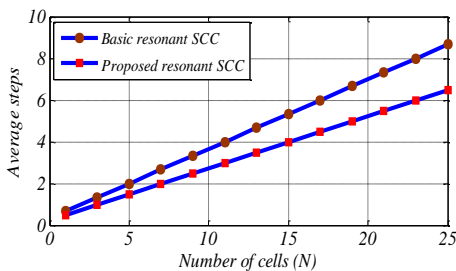
Fig. 6 Average steps for charge transfer in each converter

SIMULATION RESULTS

The proposed resonant SCC has been simulated at 50 kHz for three battery cells to compare it with the conventional converter. For the proposed converter the upper cell has an unbalanced voltage equal to 3.56 V, and the other cells' voltages are 3.28 V. So, their voltage difference is equal to 280 mV. In the dynamic model, batteries are considered as series combination of large capacitors (50 mF) and a small resistor (2 mΩ). The converter key parameters are given in table III.

TABLE III. KEY PARAMETERS OF THE CONVERTER

Parameter	Value
Frequency	50 kHz
Equivalent resistance, R_C	12 mΩ
Battery capacitance	50 mF
Resonant capacitor	1 μF
Resonant inductor	10 μH

The simulation results for two converters have been plotted in Fig. 7 to compare balancing speed of the converters. For a given specified time value equal to 10 ms, differences between maximum and minimum voltages are equal to 49 mV and 19 mV respectively for the conventional and proposed circuit.
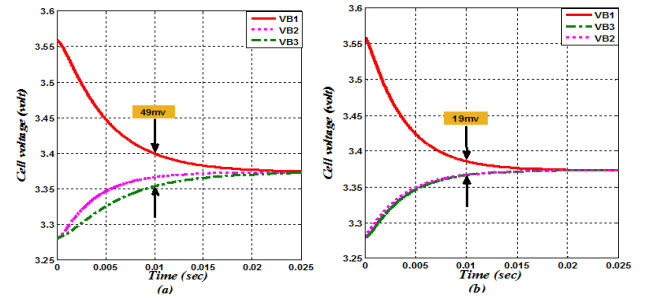
Fig. 7 MATLAB simulation results for two converters, (a) conventional and (b) proposed.

Thus, the balancing speed of the proposed converter is very higher than the conventional one. These voltage differences are compared versus balancing time in Fig. 8. To achieve less than 50 mV voltage difference, 10 ms and 7 ms are respectively necessary for the conventional and proposed converters.
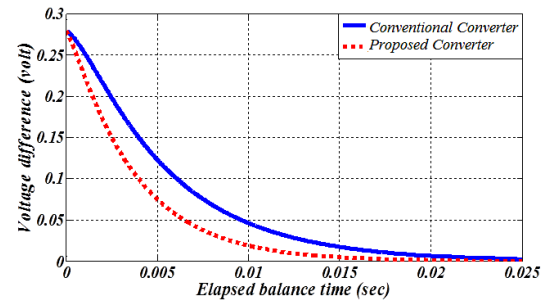
Fig. 8 Comparison between voltages differences versus time

Balancing time and power rating of the proposed converter have been plotted in Figs. 9 and versus resonant capacitor and resonant inductor values, respectively. Although, increasing the resonant capacitor value reduces balancing time and increases power rating, but, using higher values of the resonant inductor increases the balancing time and decreases the power rating, as can be concluded from Figs. 9 and 10, respectively.
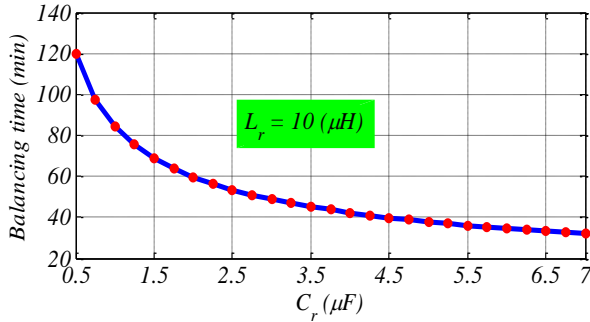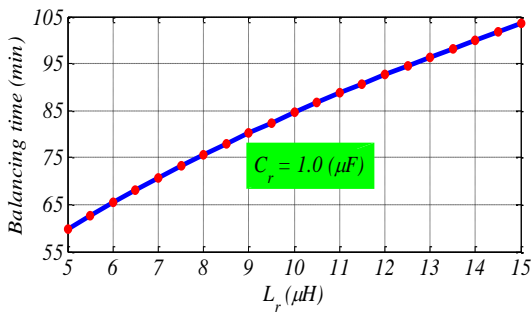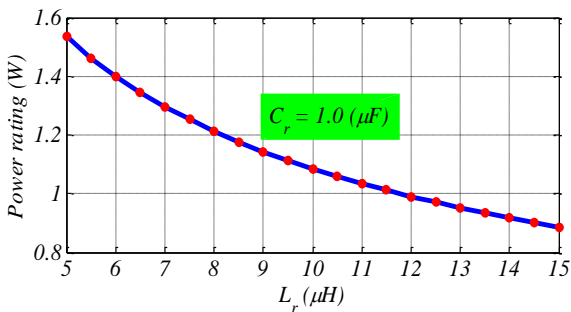

(a)
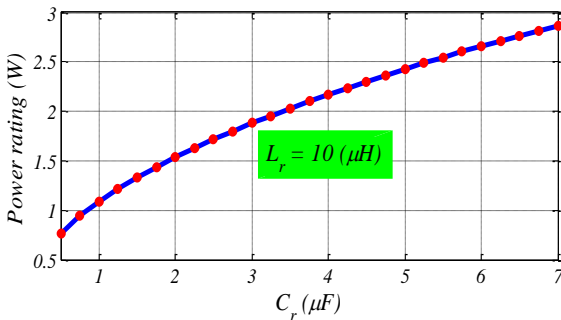
(b)

**Fig. 9** Simulation result versus C_r: (a) balancing time and (b) power rating

(a)

(b)

Fig. 10 Simulation result versus L_r: (a) balancing time and (b) power rating

Simulated efficiency curves have been plotted versus power rating in Fig. 11 for some values of the resonant tank circuit equivalent series resistance. The converter efficiency value is decreased by increasing its power rating, especially for large equivalent resistance and power rating values, as illustrated in Fig. 11.
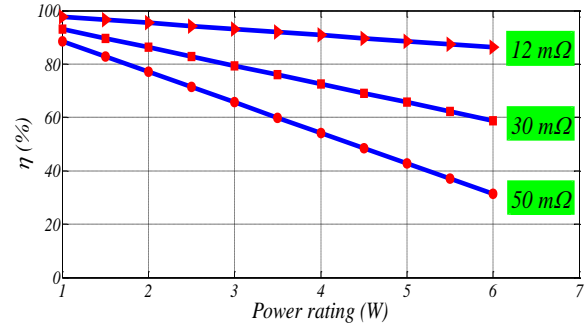

**Fig. 11** Simulated efficiency curves versus power rating

EXPERIMENTAL RESULTS

To verify the given mathematical and simulation analyses, a prototype converter has been implemented, as illustrated in Fig. 12. The balancing converter has been controlled based on an ARM-CORTEX-ST/32F407 digital controller. Its control program has been written by C programming language in IAR Embedded Workbench. To compare balancing speed of the proposed and conventional converters, maximum and minimum values of the voltage differences have been measured, as plotted in Fig. 13. After 70 minutes, 15 mV and 0.4 mV voltage differences are respectively measured for the conventional and proposed converters.
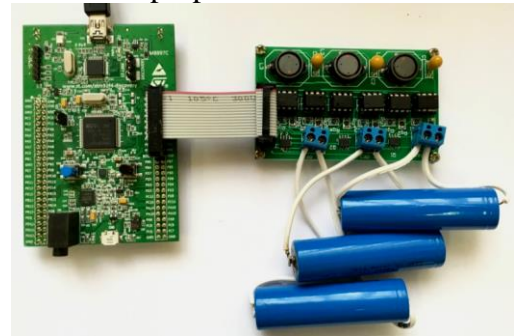
**Fig. 12** Prototype for 3 lithium-ion battery cells and experimental setup


(a)

49

(b)
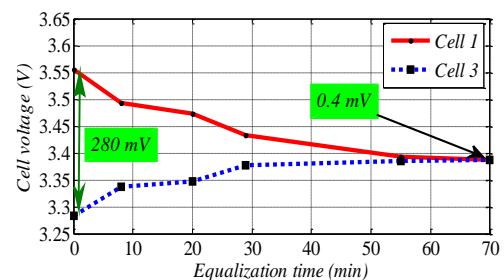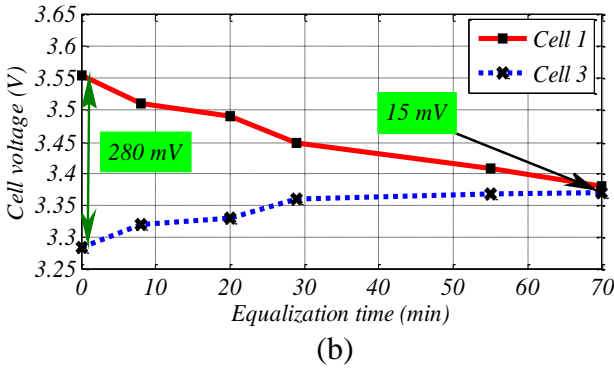
Fig.13 Experimental cells voltages versus time (a) conventional converter and (b) proposed converter

Also, a comparison between voltage differences as a function of time spent on balancing process has been done, as shown in Fig. 14 which illustrates that the proposed approach improves the balancing speed, significantly. Resonant tank's current and gate-source voltage of the third switch have been plotted in Fig. 15 to show realizing the ZCS condition at MOSFETs turn off times. But, there are some high frequency ringing on the MOSFETs currents due to their hard switching turn on events. This is a common phenomenon in the resonant SCCs that operate under the DCM conditions in their ZCS operation modes.
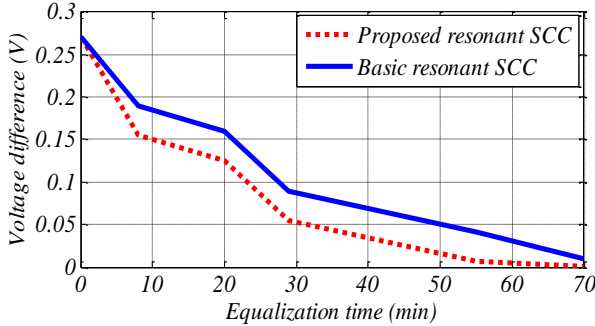
Fig.14 Comparing voltage differences of the two approaches
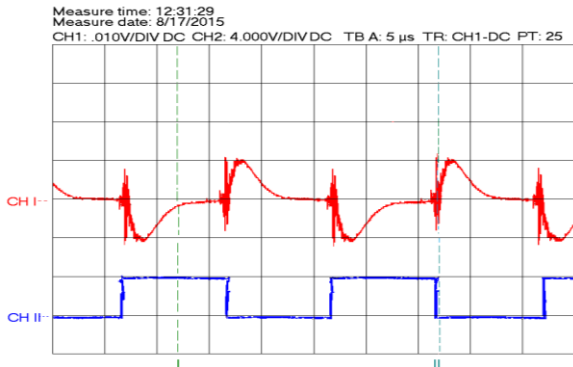
Fig. 15 Experimental waveforms of the prototype converter (up) resonant inductor current and (down) gate-source voltage

Energy efficiency is criteria for choosing a method to be effective. If the loss of charge transfer become high, the method will not be suitable. So, energy efficiency for the balance circuits is important. In reference [1], [11], two methods for calculating the energy efficiency have been presented. Energy efficiency is related to the transfer charge. However, this parameter is calculated from premised relation as follows [11]:

$$Energy\ Efficiency =$$

$$\frac{\Sigma\left(\begin{array}{c}energy\\transferred\end{array}\right) - \Sigma\left(\begin{array}{c}loss\ in\ passive\\element\end{array}\right)}{\Sigma\left(\begin{array}{c}energy\\transferred\end{array}\right)} \quad (55)$$

In the balance circuits, energy efficiency is defined as follows [1]:

$$\eta = \frac{E_{Res.}}{E_{Im.}} = \frac{\sum_{i=1}^{N} 0.5 C_{batt} \left(V_{Bi-end}^2 - V_{min}^2\right)}{\sum_{i=1}^{N} 0.5 C_{batt} \left(V_{Bi-start}^2 - V_{min}^2\right)} \quad (56)$$

It should be noted that the controller losses are not included, here. From (56), energy efficiency for both conventional and proposed methods have been depicted versus elapsed balance time in Fig. 16 which shows that efficiencies of both approaches are the same. Controller has considerable losses due to lot of switches that must be turned on and off [1], [4]. Increasing the balance speed reduces the energy loss in all controllers. Therefore, the proposed converter has high efficiency due to its high balance speed.
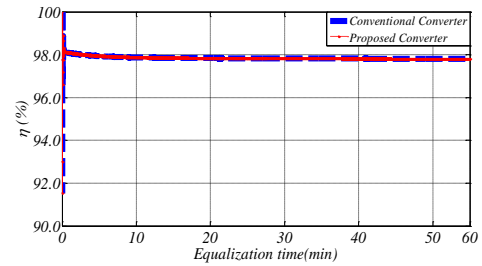
Fig.16 comparing two converters efficiency values

VII. CONCLUSION

To achieve high balancing speed and soft switching under the ZCS condition, a chain structure resonant SCC has been modified. Its different operation modes have been introduced and analyzed, mathematically. Besides, effects of the resonant tank's components on the balancing time and power rating have been investigated, in details. It has been proved that balancing speed can be improved by increasing the capacitance of the resonant capacitor and decreasing the inductor value, and vice versa. Moreover, increasing the power rating decreases the efficiency of the converter. The proposed approach improves the battery cells balancing speed more than three-fold, as compared to the conventional converter.

REFFERENCES

[1]. Kim, Moon-Young, et al. "A chain structure of switched capacitor for improved cell balancing speed of lithium-ion batteries." *Industrial Electronics, IEEE Transactions on* 61.8 (2014): 3989-3999.

[2]. Lee, Kyung-min, Yoo-chae Chung, Chang-Hyeon Sung, and Bongkoo Kang. "Active Cell Balancing of Li-Ion Batteries using LC Series Resonant Circuit." *2015 IEEE*. IEEE

[3]. Wilkins, Steven, et al. "Optimised battery capacity utilisation within Battery Management Systems." *Ecological Vehicles and Renewable Energies (EVER), 2015 Tenth International Conference on*. IEEE, 2015.

[4]. Kim, Moon-Young, et al. "A new cell-to-cell balancing circuit with a center-cell concentration structure for series-connected batteries." *ECCE Asia Downunder (ECCE Asia), 2013 IEEE*. IEEE, 2013.

[5]. Phung, Thanh Hai, Alvaro Collet, and Jean-Christophe Crebier. "An optimized topology for next-to-next balancing of series-connected lithium-ion cells." *Power Electronics, IEEE Transactions on* 29.9 (2014): 4603-4613.

[6]. Kim, Moon-Young, Jun-Ho Kim, and Gun-Woo Moon. "Center-cell concentration structure of a cell-to-cell balancing circuit with a reduced number of switches." *Power Electronics, IEEE Transactions on* 29.10 (2014): 5285-5297.

[7]. Yuanmao, Ye, K. W. E. Cheng, and Y. P. B. Yeung. "Zero-current switching switched-capacitor zero-voltage-gap automatic equalization system for series battery string." Power Electronics, IEEE Transactions on 27.7 (2012): 3234-3242.

[8]. Daowd, Mohamed, et al. "Passive and active battery balancing comparison based on MATLAB simulation." Vehicle Power and Propulsion Conference (VPPC), 2011 IEEE. IEEE, 2011.

[9]. Emadi, Ali, Young Joo Lee, and Kaushik Rajashekara. "Power electronics and motor drives in electric, hybrid electric, and plug-in hybrid electric vehicles." Industrial Electronics, IEEE Transactions on 55.6 (2008): 2237-2245.

[10]. Active Cell Balancing Methods for Li-Ion Battery Management ICs using the ATA6870.

[11]. Baughman, Andrew C., and Mehdi Ferdowsi. "Double-tiered switched-capacitor battery charge equalization technique." Industrial Electronics, IEEE Transactions on 55.6 (2008): 2277-2285.

[12]. Park, Hong-Sun, et al. "Two-stage cell balancing scheme for hybrid electric vehicle Lithium-ion battery strings." Power Electronics Specialists Conference, 2007. PESC 2007. IEEE. IEEE, 2007.

[13]. Lee, Yuang-Shung, and Guo-Tian Cheng. "Quasi-resonant zero-current-switching bidirectional converter for battery equalization applications." Power Electronics, IEEE Transactions on 21.5 (2006): 1213-1224.

[14]. Kuhn, Brian T., Grant E. Pitel, and Philip T. Krein. "Electrical properties and equalization of lithium-ion cells in automotive applications." Vehicle Power and Propulsion, 2005 IEEE Conference. IEEE, 2005.

[15]. Park, H.S., Kim, C.E., Kim, C.H., Moon, G.W. and Lee, J.H., 2009. A modularized charge equalizer for an HEV lithium-ion battery string. *Industrial Electronics, IEEE Transactions on*, 56(5), pp.1464-1476.

[16]. Einhorn, M., Guertlschmid, W., Blochberger, T., Kumpusch, R., Permann, R., Conte, F.V., Kral, C. and Fleig, J., 2011. A current equalization method for serially connected battery cells using a single power converter for each cell. *Vehicular Technology, IEEE Transactions on*, 60(9), pp.4227-4237.

[17]. Kim, Moon-Young, Chol-Ho Kim, Shin-Young Cho, and Gun-Woo Moon. "A cell selective charge equalizer using multi-output converter with auxiliary transformer." In *Power Electronics and ECCE Asia (ICPE & ECCE), 2011 IEEE 8th International Conference on*, pp. 310-317. IEEE, 2011.

[18]. Lee, W.C. and Drury, D., 2013. Development of a hardware-in-the-loop simulation system for testing cell balancing circuits. *Power Electronics, IEEE Transactions on*, 28(12), pp.5949-5959.

[19]. Uno, Masatoshi, and Kiyoshi Tanaka. "Single-switch multioutput charger using voltage multiplier for series-connected lithium-ion battery/supercapacitor equalization." *Industrial Electronics, IEEE Transactions on* 60, no. 8 (2013): 3227-3239.

[20]. Momayyezan, M., Hredzak, B. and Agelidis, V.G., 2016. Integrated Reconfigurable Converter Topology for High-Voltage Battery Systems. *Power Electronics, IEEE Transactions on*, 31(3), pp.1968-1979.

[21]. Uno, M. and Kukita, A., 2015. Bidirectional PWM Converter Integrating Cell Voltage Equalizer Using Series-Resonant Voltage Multiplier for Series-Connected Energy Storage Cells. *Power Electronics, IEEE Transactions on*, 30(6), pp.3077-3090.

[22]. Phung, T.H., Collet, A. and Crebier, J.C., 2014. An optimized topology for next-to-next balancing of series-connected lithium-ion cells. *Power Electronics, IEEE Transactions on*, 29(9), pp.4603-4613.

[23]. Young, C.M., Chu, N.Y., Chen, L.R., Hsiao, Y.C. and Li, C.Z., 2013. A single-phase multilevel inverter with battery balancing. *Industrial Electronics, IEEE Transactions on*, 60(5), pp.1972-1978.

[24]. Nguyen, Ngoc, Sai Kiran Oruganti, Kyungmin Na, and Franklin Bien. "An adaptive backward control battery equalization system for serially connected lithium-ion battery packs." *Vehicular Technology, IEEE Transactions on* 63, no. 8 (2014): 3651-3660.

[25]. Kim, M.Y., Kim, J.H. and Moon, G.W., 2014. Center-cell concentration structure of a cell-to-cell balancing circuit with a reduced number of switches. *Power Electronics, IEEE Transactions on*, *29*(10), pp.5285-5297.

[26]. Park, S.H., Park, K.B., Kim, H.S., Moon, G.W. and Youn, M.J., 2012. Single-magnetic cell-to-cell charge equalization converter with reduced number of transformer windings. *Power Electronics, IEEE Transactions on*, *27*(6), pp.2900-2911.

[27]. Park, H.S., Kim, C.E., Moon, G.W., Lee, J.H. and Oh, J.K., 2007, June. Two-stage cell balancing scheme for hybrid electric vehicle Lithium-ion battery strings. In *Power Electronics Specialists Conference, 2007. PESC 2007. IEEE* (pp. 273-279). IEEE.

[28]. Kreins, C. Pascual PT. "Switched capacitor system for automatic series battery equalization." In *Proceedings of IEEE Applied Power Electronics Conference*, pp. 23-27. 1997.

[29]. Uno, Masatoshi, and Koji Tanaka. "Single-switch cell voltage equalizer using multistacked buck-boost converters operating in discontinuous conduction mode for series-connected energy storage cells." *Vehicular Technology, IEEE Transactions on* 60, no. 8 (2011): 3635-3645.

[30]. Lee, Y.S. and Cheng, M.W., 2005. Intelligent control battery equalization for series connected lithium-ion battery strings. *Industrial Electronics, IEEE Transactions on*, *52*(5), pp.1297-1307.

[31]. Uno, M. and Tanaka, K., 2012. Double-switch single-transformer cell voltage equalizer using a half-bridge inverter and a voltage multiplier for series-connected supercapacitors. *Vehicular Technology, IEEE Transactions on*, *61*(9), pp.3920-3930.